

Supplementary Materials for

Spatiotemporal Imaging of Electrocatalytic Activity on Single 2D Gold Nanoplates via Electrogenerated Chemiluminescence Microscopy

Ming-Ming Chen, ‡ Wei Zhao, ‡ Meng-Jiao Zhu, Xiang-Ling Li, Cong-Hui Xu,* Hong-Yuan Chen,
Jing-Juan Xu*

State Key Laboratory of Analytical Chemistry for Life Science and Collaborative Innovation Center of Chemistry for Life Sciences, School of Chemistry and Chemical Engineering, Nanjing University, Nanjing 210023, China.

*Corresponding authors. Tel/fax: +86-25-89687294. E-mail: chxu@nju.edu.cn, xujj@nju.edu.cn

‡ These authors contributed equally to the work.

Table of contents

1. Optical characterization of the gold nanoplates.....	S-3
2. The surface morphology characterization after UV/ozone treatment.....	S-3
3. The influence of CTAB to the ECL imaging.....	S-3
4. Calculation of the heterogeneous electron transfer rate constant at gold nanoplates	S-4
5. Stability of nanoplate morphology in ECL measurements.....	S-5
6. Details for digital simulation.....	S-6
• Physical field.....	S-6
• Procedure.....	S-6
• Meshes setting.....	S-8
• Simulation results.....	S-8
7. References.....	S-9

1. Optical characterization of gold nanoplates

The UV-vis absorption spectroscopy (Figure S1a) shows that the nanoplates exhibit a strong broad absorption band at about 600 nm and a weak band centered at 750~800 nm, which are in agreement with the literature report.¹ The scattering spectrum was obtained from a triangle gold nanoplate, which was centered at 654 nm and attributed to the quadrupole plasmon mode.²

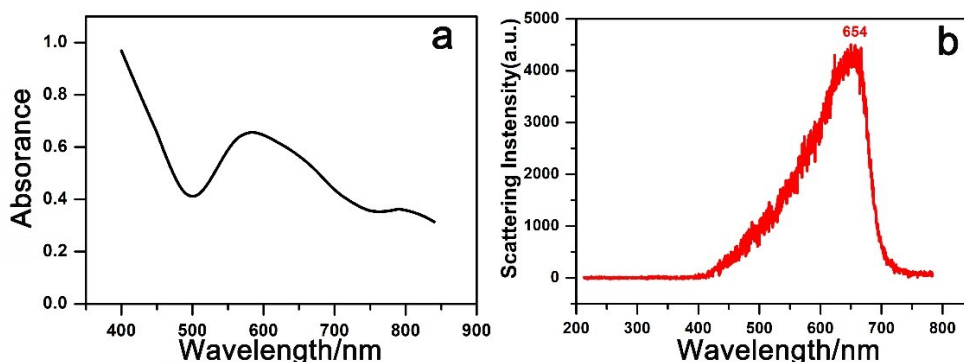


Figure S1. (a) UV-vis absorption spectrum and (b) scattering spectrum of the synthesized gold nanoplates.

2. The surface morphology characterization after UV/ozone treatment

Hexadecyltrimethylammonium bromide (CTAB) surfactant, which greatly hinders the electrochemical activity of the nanoplates was removed before ECL imaging. Here we treated the surface of nanoplates with UV/ozone, which could efficiently remove the organic components. The surface morphology of gold nanoplates was characterized before and after UV/ozone. As shown in SEM images (Figure S2), the pretreatment barely influenced the surface morphology.

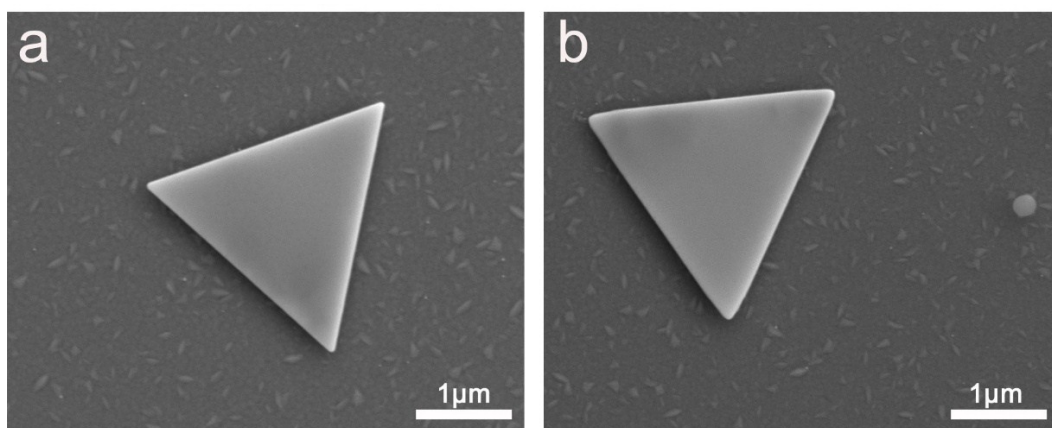


Figure S2. SEM images single gold nanoplate (a) before and (b) after UV/ozone treatment

3. The influence of the CTAB ligands to the ECL imaging

Figure S3 compares the bright-field microscopy images and the corresponding ECL images before and after UV/ozone treatment. As shown in panel b, no ECL signal was observed at the CTAB coated gold nanoplates, suggesting that the bulky stabilizing ligand blocked the electron transfer and prevented ECL signal. On the other hand, after removing CTAB from the surface of nanoplates, ECL produced at the gold nanoplates with high resolution, and the positions of ECL spots fitted perfectly with those from bright-field image (panels c and d).

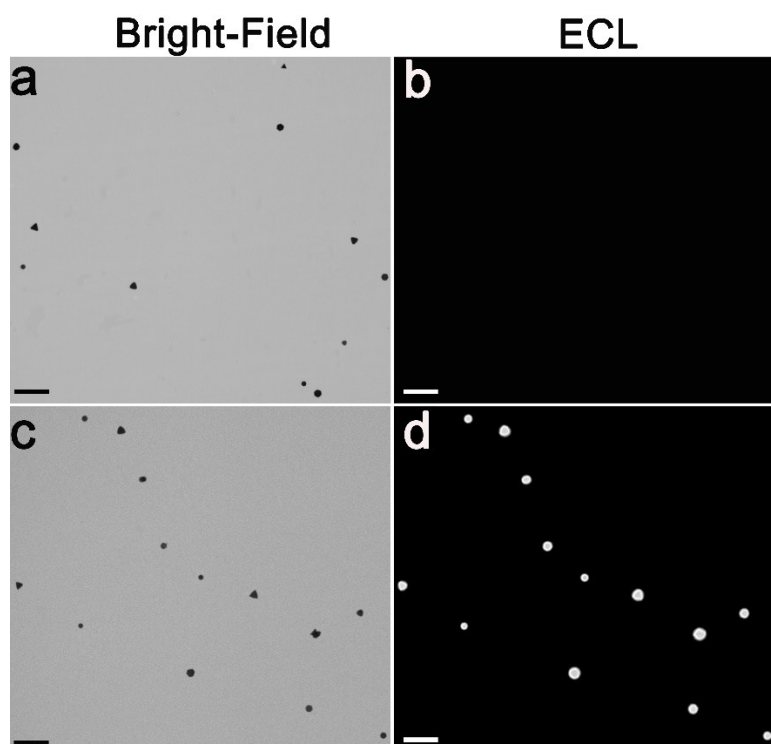


Figure S3. Bright-field (left column) and corresponding ECL (right column) images of gold nanoplates with potential stepped to +1.2 V vs. Ag/AgCl (a, b) before and (c, d) after UV/ozone treatment. All samples were immersed in 10 mM phosphate buffer containing 1 mM Ru(bpy)₃²⁺, 20 mM TPrA at pH 7.2. Scar bar: 20 μm.

4. Calculation of the heterogeneous electron transfer rate constant at gold nanoplates

As ECL is a electrogenerated chemiluminescence due to electrochemical redox reactions at the surface of electrode, the ECL intensity should be positively correlated to the Faradaic current.^{3, 4} To calculate the heterogeneous electron transfer rate constant k^0 at single gold nanoplates, we calibrated the ECL intensity and current density using microelectrodes with diameters from 12.5 μm to 100.0 μm. The current density (J) was calculated by $J=I/A$. Since the reactions of Ru(bpy)₃²⁺ and TPrA at the surfaces of the microelectrodes are diffusion-controlled, A is the geometric area of the electrode. As shown in Figure S4, the ECL intensity is proportional to current density resulted from Ru(bpy)₃²⁺ and TPrA (Figure S4e), and Ru(bpy)₃²⁺ (Figure S4f) alone. Based on the linear fitted equation, the heterogeneous electron transfer rate constant on single gold nanoplates could be determined.

Since the oxidation and reduction of Ru (bpy)₃^{2+/3+} redox pair is reversible, the current-potential characteristic could be described with Butler–Volmer (B-V) formalism.⁵

$$i = F A k^0 [C_O(0,t) e^{-\alpha f(E-E^0)} - C_R(0,t) e^{(1-\alpha)f(E-E^0)}] \quad (1)$$

Where F is Faraday's constant (96,485 Cmol⁻¹), A is the area of electrode, k^0 is the standard reaction rate constant, α is the transfer coefficient taking as 0.5, C_O and C_R are the concentration of oxidized Ru(bpy)₃³⁺ and reduced Ru(bpy)₃²⁺ species, $f = F/RT$ (38.92 V⁻¹, at 25 °C). The potential difference of $(E-E^0) = 140$ mV. As the ECL images were all recorded at the first potential step within 400 ms, we took the initial time ($t = 0$) of this reaction without production of C_O , and the oxidation current could be written as:

$$i_{ox} = F A k^0 C_R e^{(1-\alpha)f(E-E^0)} \quad (2)$$

C_R is the initial concentration of $\text{Ru}(\text{bpy})_3^{2+}$. On the basis of the fitted linear equation, the heterogeneous electron transfer rate constant k^0 at gold nanoplates was calculated as 0.02cm/s.

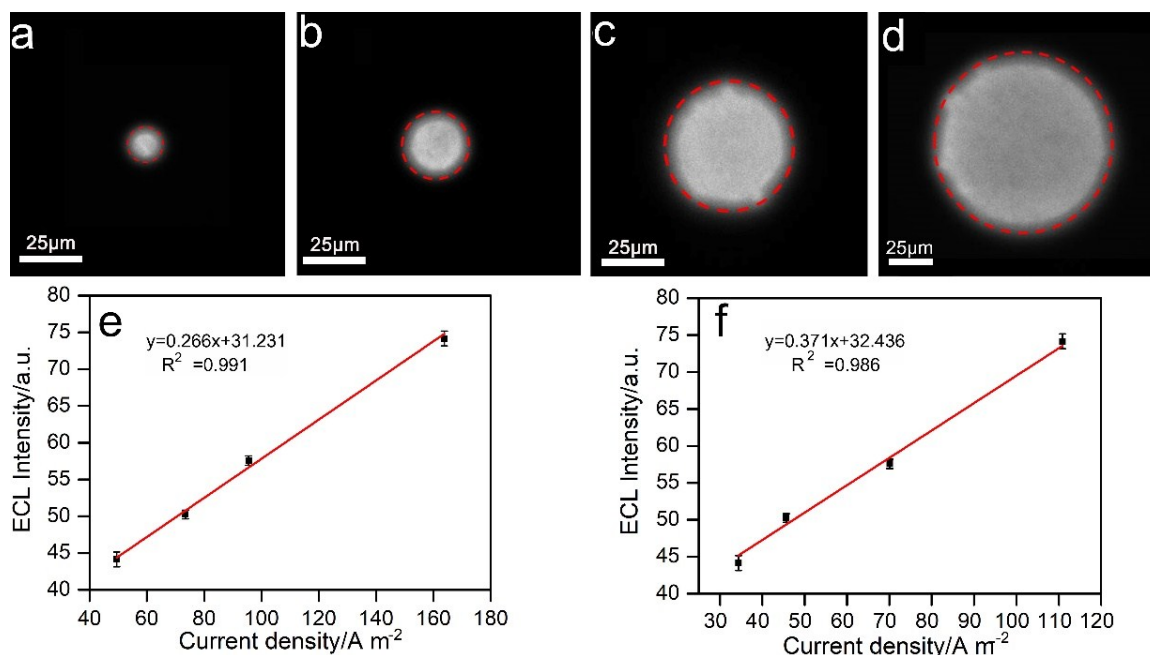


Figure S4. (a-d) ECL images of microelectrodes with diameter of 12.5 μm, 25 μm, 50 μm and 100 μm. Exposure time: 200ms. (e,f) Linear fitted relationship between ECL intensity and current densities obtained from the three-electrode system with 10 mM phosphate buffer containing (e) 1 mM $\text{Ru}(\text{bpy})_3^{2+}$ and 20 mM TPrA, and (f) 1 mM $\text{Ru}(\text{bpy})_3^{2+}$.

5. Stability of nanoplate morphology in ECL measurements

To evaluate the stability of gold nanoplates under excitation potential, bright-field images were taken before and after ECL measurements with 10 times excitation under 1.2 V vs. Ag/AgCl. As is shown in Figure S5, no dramatic morphological changes at gold nanoplates were observed, indicating that the decrease of ECL intensity after several potential steps was ascribed to the surface oxidation instead of anodic dissolution of gold in solution containing chloride ions.⁶

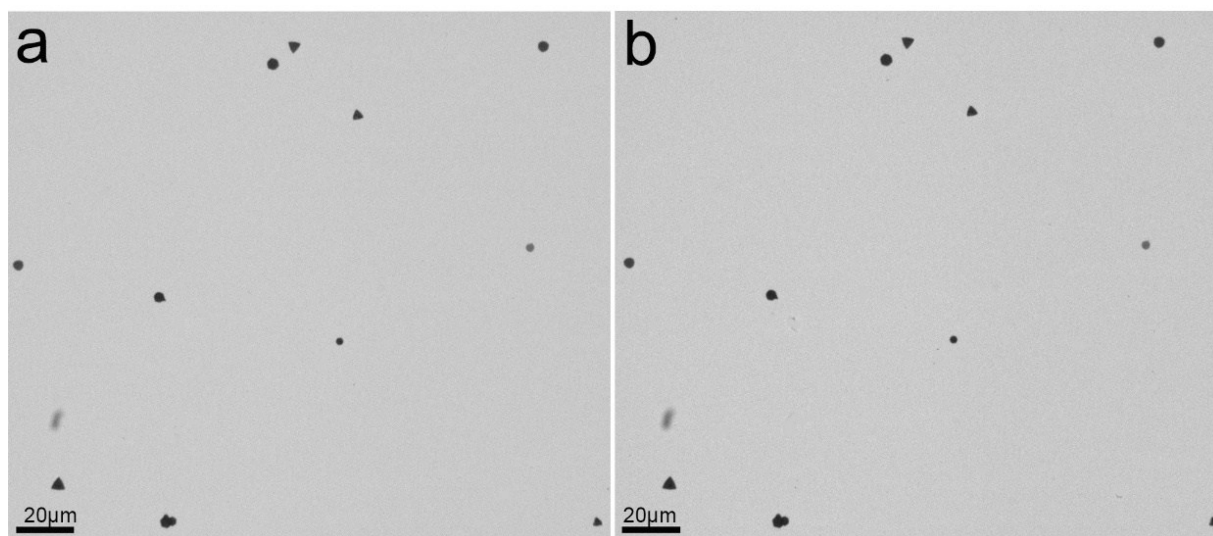


Figure S5. Bright-field images of the gold nanoplates before (a) and after (b) ten potentials steps to 1.2 V vs. Ag/AgCl.

6. Details for digital simulation

COMSOL Multiphysics 5.3a was employed to determine reaction rate and concentration profiles of different Ru ion species with three-dimensional finite element modeling.

Physical field. “Transport of Diluted Species” physical field was used for simulating ECL reactions. In the physical field, time-dependent study on transport of diluted species was used to simulate the concentration around the gold microelectrodes. The inflow of the pristine substances to the electrode and the outflow of the products to the bulk solution were described below.

$$\frac{\partial C_i}{\partial t} + \nabla \cdot (-D_i \nabla C_i) = R_i \quad (3)$$

$$N_i = -D_i \nabla C_i \quad (4)$$

Procedure. The redox reaction of $\text{Ru}(\text{bpy})_3^{2+}/\text{Ru}(\text{bpy})_3^{3+}$ is a typical one-step, one-electron process. The current-potential characteristic could be described with Butler–Volmer (B-V) formalism. In numerical simulation, the transition conditions of redox species were follow the Fick’s Second law.

$$\frac{\partial C_O}{\partial t} = D_O \nabla^2 C_O \quad (5)$$

$$\frac{\partial C_R}{\partial t} = D_R \nabla^2 C_R \quad (6)$$

Where C_O and C_R are the concentration of oxidized and reduced species, and they are the function of time and heterogeneous reaction rate k . D_O , D_R are diffusion coefficient for the oxidized and reduced species and are taken as $1 \times 10^{-5} \text{ cm}^2/\text{s}$ for all the species in the whole simulation.

The potential pulses are set at 0 V and 1.2 V with 400 ms time interval (2.5 Hz). At potential of 1.2 V vs. Ag/AgCl, 12 reactions could be involved in the ECL response (Table S1).

Table S1. ECL reactions and parameters.

Electrochemical redox reactions	$E^0(\text{V})$ vs. Ag/AgCl	$k_0(\text{cm/s})$
(1) $\text{Ru}(\text{bpy})_3^{3+} + e^- \xrightarrow{k_1} \text{Ru}(\text{bpy})_3^{2+}$	1.06	0.02
(2) $\text{TPrA}^{\cdot+} + e^- \xrightarrow{k_2} \text{TPrA}$	0.90	0.6
(3) $\text{P} + e^- \xrightarrow{k_3} \text{TPrA}^{\cdot}$	≤ 1.7	\
Homogeneous Reactions		k_f
(4) $\text{TPrA}^{\cdot+} \xrightarrow{k_4} \text{TPrA}^{\cdot} + \text{H}^+$		$537(\text{s}^{-1})$
(5) $\text{HA} \xrightarrow{k_5} \text{H}^+ + \text{A}^-$		$6.3 \times 10^{-8}(\text{M}^{-1}\text{s}^{-1})$
(6) $\text{TPrA} + \text{HA} \xrightarrow{k_6} \text{A}^- + \text{TPrAH}$		$6.3 \times 10^{-9}(\text{M}^{-1}\text{s}^{-1})$
(7) $\text{Ru}(\text{bpy})_3^{2+} + \text{TPrA}^{\cdot} \xrightarrow{k_7} \text{Ru}(\text{bpy})_3^{3+} + \text{P}$		$10^{10}(\text{M}^{-1}\text{s}^{-1})$
(8) $\text{Ru}(\text{bpy})_3^{2+} + \text{Ru}(\text{bpy})_3^{3+} \xrightarrow{k_8} \text{Ru}(\text{bpy})_3^{2+*} + \text{Ru}(\text{bpy})_3^{2+}$		$10^{10}(\text{M}^{-1}\text{s}^{-1})$

(9) $\text{Ru}(\text{bpy})_3^{3+} + \text{TPrA} \xrightarrow{k_9} \text{TPrA}^{\cdot+} + \text{Ru}(\text{bpy})_3^{2+*}$	1 ($\text{M}^{-1}\text{s}^{-1}$)
(10) $\text{Ru}(\text{bpy})_3^{3+} + \text{TPrA}^{\cdot+} \xrightarrow{k_{10}} \text{Ru}(\text{bpy})_3^{2+*} + \text{P}$	$10^{10}(\text{M}^{-1}\text{s}^{-1})$
(11) $\text{Ru}(\text{bpy})_3^{3+} + \text{TPrA}^{\cdot+} \xrightarrow{k_{11}} \text{Ru}(\text{bpy})_3^{2+*} + \text{TPrA}$	$10^6(\text{M}^{-1}\text{s}^{-1})$
(12) $\text{Ru}(\text{bpy})_3^{2+*} \xrightarrow{k_{12}} \text{Ru}(\text{bpy})_3^{2+} + \text{h}\nu$	$10^{7.2}(\text{s}^{-1})$

(Notes: P stands for TPrA loses two electrons and one proton. HA means H_2PO_4 . All the parameters are from the previous paper ⁷)

Reactions 1, 2, 4, 7, 8 and 12 were considered in numerical simulation. In this simulation, all redox and intermediate species are assumed to have no adsorption onto the nanoplates, their mass transfer coefficients remain the same as those in bulk solution near the particles. The initial concentration of $\text{Ru}(\text{bpy})_3^{2+}$ and TPrA are 1 mM and 20 mM respectively. Other parameters for simulations: $R=8.31 \text{ J}/(\text{kmol})$, $T=298 \text{ K}$, $F=96485 \text{ C}/\text{mol}$, $f = F/RT=38.92 \text{ V}^{-1}$.

Table S2. Heterogeneous reaction rates of $\text{Ru}(\text{bpy})_3^{2+/3+}$ and TPrA/TPrA^{·+} redox reactions

	Expression	Value
k_1 (cm/s)	-	0.02
k_2 (cm/s)	-	0.6
k_f (m/s)	$k_0 \times \exp(-0.5 \times (E-1.06) \times (F/RT))$	1.31×10^{-5}
k_b (m/s)	$k_0 \times \exp(0.5 \times (E-1.06) \times (F/RT))$	3.05×10^{-3}
k_{f1} (m/s)	$k_1 \times \exp(-0.5 \times (E-0.90) \times (F/RT))$	1.75×10^{-5}
k_{b1} (m/s)	$k_1 \times \exp(0.5 \times (E-0.90) \times (F/RT))$	2.06

Table S3. The molar influxes of the $\text{Ru}(\text{bpy})_3^{2+}$, $\text{Ru}(\text{bpy})_3^{3+}$, TPrA and TPrA^{·+}

Variables	Expression	Equation	Unit
$N_{\text{Ru}(\text{bpy})_3^{2+}}$	$-D_{\text{Ru}2} \nabla C_{\text{Ru}2}$	$k_f \times \text{Ru}(\text{III}) - k_b \times \text{Ru}(\text{II})$	$\text{mol}/(\text{m}^2 \cdot \text{s})$
$N_{\text{Ru}(\text{bpy})_3^{3+}}$	$-D_{\text{Ru}3} \nabla C_{\text{Ru}3}$	$-k_f \times \text{Ru}(\text{III}) + k_b \times \text{Ru}(\text{II})$	$\text{mol}/(\text{m}^2 \cdot \text{s})$
N_{TPrA}	$-D_{\text{TPrA}} \nabla C_{\text{TPrA}}$	$k_{f1} \times \text{TPrA}^{\cdot+} - k_{b1} \times \text{TPrA}$	$\text{mol}/(\text{m}^2 \cdot \text{s})$
$N_{\text{TPrA}^{\cdot+}}$	$-D_{\text{TPrA}^{\cdot+}} \nabla C_{\text{TPrA}^{\cdot+}}$	$-k_{f1} \times \text{TPrA}^{\cdot+} + k_{b1} \times \text{TPrA}$	$\text{mol}/(\text{m}^2 \cdot \text{s})$

Table S4. In the electrolyte (domain), the concentration change of the involved species with time

Chemical	Expression	Unit
$\text{Ru}(\text{bpy})_3^{2+}$	$\frac{\partial \text{Ru}(\text{II})}{\partial t} = D \nabla^2 C_{\text{Ru}(\text{II})} - k_7 \times \text{Ru}(\text{II}) \times \text{TPrA}$ $+ k_8 \times \text{Ru}(\text{I}) \times \text{Ru}(\text{III}) + \text{Ru}^* \times k_{12}$	$\text{mol}/(\text{m}^3 \cdot \text{s})$
$\text{Ru}(\text{bpy})_3^{3+}$	$\frac{\partial \text{Ru}(\text{III})}{\partial t} = D \nabla^2 C_{\text{Ru}(\text{III})} - k_8 \times \text{Ru}(\text{I}) \times \text{Ru}(\text{III})$	$\text{mol}/(\text{m}^3 \cdot \text{s})$

$\text{Ru}(\text{bpy})_3^{2+*}$	$\frac{\partial \text{Ru}(I)}{\partial t} = D\nabla^2 C_{\text{Ru}(I)} + k_7 \times \text{Ru(II)} \times \text{TPrA} \cdot - k_8 \times \text{Ru(I)} \times \text{Ru(III)}$	mol/(m ³ .s)
$\text{Ru}(\text{bpy})_3^{2+}$	$\frac{\partial \text{Ru}^*}{\partial t} = D\nabla^2 C_{\text{Ru}^*} + k_8 \times \text{Ru(I)} \times \text{Ru(III)} - \text{Ru}^* \times k_{12}$	mol/(m ³ .s)
TPrA	$\frac{\partial \text{TPrA}}{\partial t} = D\nabla^2 C_{\text{TPrA}}$	mol/(m ³ .s)
$\text{TPrA} \cdot^+$	$\frac{\partial \text{TPrA} \cdot^+}{\partial t} = D\nabla^2 C_{\text{TPrA} \cdot^+} - k_4 \times \text{TPrA} \cdot^+$	mol/(m ³ .s)
$\text{TPrA} \cdot$	$\frac{\partial \text{TPrA} \cdot}{\partial t} = D\nabla^2 C_{\text{TPrA} \cdot} + k_4 \times \text{TPrA} \cdot^+ - k_7 \times \text{Ru(II)} \times \text{TPrA} \cdot$	mol/(m ³ .s)

Meshes setting. The mesh setting was extremely fine. The minimum element size is 5×10^{-9} m of the gold plates.

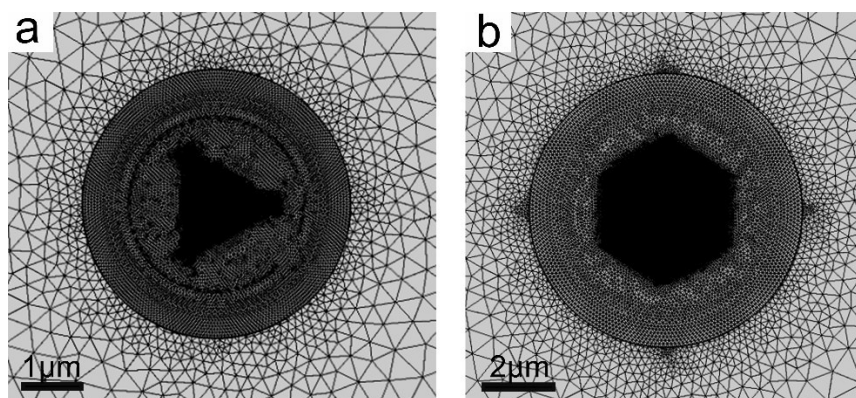


Figure S6. Mesh setting of a) the triangle and b) hexagon gold plates.

Simulation results. We tried to change the parameters in COMSOL simulation and it was found out that the lifetime of the excited $\text{Ru}(\text{bpy})_3^{2+*}$ had great impact on its concentration profile. We varied the decay rate of $\text{Ru}(\text{bpy})_3^{2+*}$ to 10^4 s^{-1} in 3D COMSOL simulation. Simulated ECL profile shows gradient with flat facets > perimeter on both triangle and hexagon gold plates (Figure S7). On the other hand, with 10^{10} s^{-1} decay rate, the ECL distribution is the opposite (Figure S8). With longer lifetime, the distribution of $\text{Ru}(\text{bpy})_3^{2+*}$ is greatly influenced by the edge dominated flux. Therefore, although more excited species are generated at the edges, the higher flux could result in lower concentration.

Concentration Distribution of $h\nu_{\text{ECL}}$

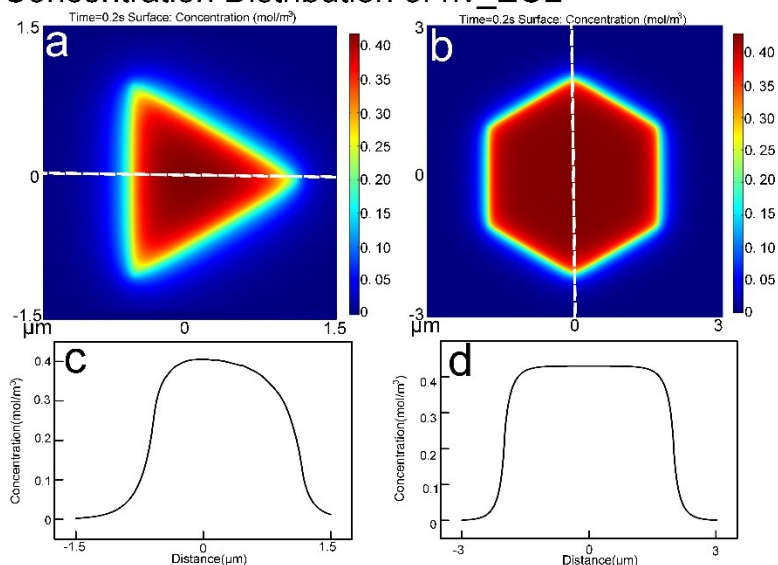


Figure S7. The concentration distributions of ECL intensity on the (a) the triangle and (b) hexagon gold nanoplates with radiative decay rate as 10^4 s^{-1} . Figure c, d represent the ECL distribution across measuring line marked in a and b.

Concentration Distribution of $h\nu_{\text{ECL}}$

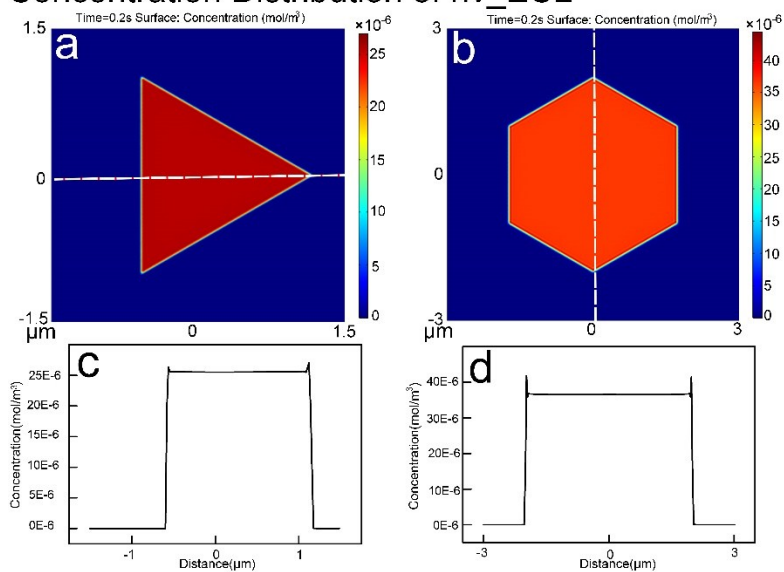


Figure S8. The concentration distributions of ECL intensity on the (a) the triangle and (b) hexagon gold nanoplates with radiative decay rate as 10^{10} s^{-1} . Figure c, d represent the ECL distribution across measuring line marked in a and b.

7. References

1. W.-L. Huang, C.-H. Chen and M. H. Huang, *J. Phys. Chem. C*, 2007, **111**, 2533-2538.
2. J. E. Millstone, S. Park, K. L. Shuford, L. Qin, G. C. Schatz and C. A. Mirkin, *J. Am. Chem. Soc.*, 2005, **127**, 5312-5313.
3. F. Kanoufi, Y. Zu and A. J. Bard, *J. Phys. Chem. B*, 2001, **105**, 210-216.
4. C. M. Pharr, R. C. Engstrom, R. A. Tople, T. K. Bee and P. L. Unzelman, *J. Electroanal. Chem. Interfacial Electrochem.*, 1990, **278**, 119-128.

5. A. J. Bard, L. R. Faulkner, J. Leddy, C. G. Zoski, *Electrochemical Methods: Fundamentals and Applications*, Vol. 2, Wiley, New York, 1980.
6. J. H. Gallego, C. E. Castellano, A. J. Calandra and A. J. Arvia, *J. Electroanal. Chem. Interfacial Electrochem.*, 1975, **66**, 207-230.
7. R. M. Wightman, S. P. Forry, R. Maus, D. Badocco and P. Pastore, *J. Phys. Chem. B*, 2004, **108**, 19119-19125.